Galactic Cosmic Rays Access to the Magnetosphere of Saturn

Anna Kotova, E. Roussos, P. Kollmann, N. Krupp, I. Dandouras

Galactic Cosmic Rays access to the magnetosphere of Saturn

A. Kotova[1], E. Roussos[2], P. Kollmann[3], N. Krupp[2], and I. Dandouras[1]

Anna Kotova, akotova@irap.omp.eu

[1]IRAP, Université de Toulouse, CNRS,

CNES, UPS, Toulouse, France

[2]Max Planck Institute for Solar System

Research, Justus-von-Liebig-Weg 3,

Göttingen, 37077, Germany

[3]Johns Hopkins University Applied

Physics Laboratory, Laurel MD 20723-6099,

USA

This article has been accepted for publication and undergone full peer review but has not been through the copyediting, typesetting, pagination and proofreading process, which may lead to differences between this version and the Version of Record. Please cite this article as doi: 10.1029/2018JA025661

Abstract.

The MeV proton radiation belts of Saturn are isolated from the middle and outer magnetosphere and the source of these high energy protons is thought to be linked to the access of Galactic Cosmic Rays (GCRs) in the system. To validate this hypothesis it is first of all necessary to determine the realistic spectrum of GCRs at Saturn. Previously only analytical attempts were performed in order to calculate the GCR spectra. In this letter we provide for the first time the numerical solution for the determination of the GCR access to the upper atmosphere and rings of Saturn. The proposed method is based on the charged particle tracing technique. As a result the GCRs access energies to the atmosphere and to the equatorial plane of the magnetosphere as a function of radial distance to the planet were obtained and the GCRs spectra were reconstructed. Dependencies of the spectral parameters such as the time or the incidence direction, were also obtained offering all necessary information for simulating the interaction of GCRs with the saturnian system during different phases of the Cassini mission.

Keypoints:

- We provide GCR access energies to the Saturnian atmosphere and across the magnetosphere
- GCR spectra and integrated flux to Saturn and to the equatorial plane of the magnetosphere are calculated
- Advantages of a particle tracing approach over the analytical solution are demonstrated

1. Introduction

The presence of stable radiation belts of Saturn between the outer edge of the A ring (2.27 R_S, where R_S is the radius of Saturn) and Tethys' orbit (4.8 R_S) was confirmed already during the first visits of this planet by Pioneer 11, Voyager 1 and 2 [*Fillius et al.*, 1980; *Krimigis and Armstrong*, 1982; *Simpson et al.*, 1980; *Vogt et al.*, 1982]. Rings and numerous moons of Saturn shape the unique configuration of the Saturnian radiation belts. Bouncing between mirror points the energetic charged particles regularly cross the equatorial plane of the magnetosphere. Owing to the nearly symmetric magnetic field and their almost circular and equatorial orbits, the large moons of Saturn effectively absorb the trapped energetic particles that follow the magnetic field lines of those moons' L-shells along their motion around the planet. These sweeping corridors that form behind the moons barely replenish, indicating that radial diffusion cannot supply the radiation belts with a sufficient portion of new energetic particles from the middle magnetosphere. Cassini observations confirmed, that energetic ions along these L-shells are absent in all magnetospheric local times and latitudes, independently from the location of the moons. Similarly absorption of the charged particles happens along the L-shells connected to the Main Rings. In the same time, outside the Tethys orbit proton fluxes are changing a lot from one orbit to another, but the particle flux inside the radiation belts remains unchanged [*Roussos et al.*, 2008; *Paranicas et al.*, 2008]. Independently from the solar cycle phase only a weak modulation on the time scale of years was observed by Cassini MIMI/LEMMS in the $>$ 10 MeV protons flux of the Saturnian radiation belts [*Roussos*

et al., 2011; *Kollmann et al.*, 2017].

This indicated that the source for these energetic ions should be local, most likely being connected to the interaction of Galactic Cosmic Rays (GCR) with Saturn and its rings through the CRAND (Cosmic Ray Albedo Neutron Decay) process [*Blake et al.*, 1983; *Cooper*, 1983; *Cooper et al.*, 1985]. Existence of the energetic protons population within Saturn's innermost radiation belt, located in the narrow zone between the Saturn's atmosphere and the Main Rings, was recently confirmed during Cassini Proximal orbits in 2017. This population can originate also only from CRAND [*Roussos et al.*, 2018a; *Kollmann et al.*, 2018].

At Saturn this process was described by several authors including *Fillius et al.* [1980]; *Cooper* [1983]; *Fillius and McIlwain* [1980]; *Van Allen et al.* [1980]; *Randall* [1994]; *Kollmann et al.* [2013]. A GCR proton with a sufficient energy enters the magnetosphere, reaches the planet and undergoes collisions with atmospheric particles or ring matter and produces cascades of secondaries, also known as *cosmic ray showers*. These secondaries include neutrons, protons, electrons, neutrinos, pions, muons, various antiparticles and photons, partly at much lower energies. Charged secondary particles will be trapped by the magnetic field and most probably will be absorbed during their bounce motion in a short time. Neutrons in contrast can freely escape from their production region. A free neutron has a mean lifetime of 885.7 ± 0.8 sec [*Nakamura and Group*, 2010]. Beta decay of a neutron leads to the production of a proton, an electron and an electron antineutrino.

The difference in atomic mass of neutron and proton leads to the release of 782 keV of the kinetic energy, which is shared between the electron and the antineutrino, and all the kinetic energy of a parent neutron goes to the daughter proton [*Blake et al.*, 1983]. Energetic (keV-GeV) neutrons decay with low probability inside the magnetosphere across a wide range of L-shells and thus populate the radiation belts with a newborn energetic proton and electron.

In order to estimate the CRAND input on the radiation belts population it is essential first of all to determine the incoming GCR flux onto the Saturnian atmosphere and rings. Saturn has a strong magnetic field which can deflect high energy GCRs. However, if the GCR has enough energy, it still can get into the atmosphere (or on the planetary rings). Therefore, for any given location and arrival direction it is necessary to determine an energy, which can overcome the deflection by the planetary magnetic field and reach the atmosphere (or rings). We will name this energy "*access energy*".

There exist analytical and numerical solutions for its determination. However most of them were developed for Earth and do not take into account the specificities of other planets, such as their non-dipolar magnetic field. Particularly for Saturn only analytical calculations were performed so far by the above-mentioned authors, providing uncertain results. Therefore the comprehensive study of the CRAND process at Saturn essentially requires using a numerical method is essential.

In this work we use particle tracing to determine the incoming GCR flux at a given location. This method can provide a solution for many different questions in the study of the GCR impact on the magnetosphere of Saturn.

2. Analytical Solution Versus Tracing Technique

2.1. Analytical Solution Based on Störmer Theory

The Störmer theory for the calculation of the particle's energy needed to access the planetary surface (or atmosphere) is based on the concept of *magnetic rigidity*, which describes the resistance of a charged particle to change its direction of motion under the influence of a magnetic force [*Kallenrode*, 2004]. Similarly the GCR *cutoff rigidity* is a quantitative measure of planetary magnetic field shielding [*Smart and Shea*, 2005] and is proportional to the momentum needed for a cosmic ray to reach the planet at a specific location as a function of arrival direction (see the Support Information for formulas).

The analytical approach is a relatively fast method for the derivation of the GCR cutoff energy and can be sufficient as a first approximation for some problems, but cannot sustain an accurate and precise solution. Analytically derived values for GCR access energies do not fit the observed ones at Earth, because the real planetary magnetic field is not a static dipole magnetic field and because the planetary magnetosphere is deformed by a series of processes changing its shape with solar wind conditions.

Satellite observations show a marked variation of the detected GCR flux with changes of the magnetic activity within a magnetosphere and suggest that the GCR access energy

decreases as the magnetic activity increases [*Reid and Sauer*, 1967]. The dipole model lacks the higher order moments (quadrupole, octopole, etc.) of the magnetic field, which makes a significant difference for the GCR access energies at lower latitudes and at higher energies [*Weygand and Raeder*, 2005; *Beer et al.*, 2012]. Since the contributions of higher order moments of the magnetic field vary as a function of space and time, the GCR cutoff energy varies correspondingly.

Various currents in the magnetosphere, especially the ring current and the cross-tail current, are important contributors to the decrease of the cutoff energies, compared to analytically calculated values [*Reid and Sauer*, 1967; *Dorman*, 2009]. The complex shape of the magnetosphere influences the GCR access and in particular, certain particles with lower energy still can access the planet through the tail.

Compression of the magnetosphere under the changing solar wind conditions and during extreme coronal mass ejections [*Adriani et al.*, 2016], solar modulation of the GCR flux in the Solar system, related to the solar cycle, seasonal changes in the magnetosphere along the motion of the planet around the Sun and other periodical changes of the conditions in the magnetosphere and in the ambient GCR flux are all reflected in the final dose of GCR reaching the planet.

Moreover, particularly at Saturn, the presence of rings plays an important role: GCRs can pass through Saturn's rings. While the rings are not massive enough to be an obstacle for the entire GCR flux, they contain large enough bodies, which could be hit by the

GCRs producing secondaries showers and such a passage would drive the CRAND process. All these factors cannot be taken into account in an analytical formula. In contrast, the trajectory tracing method can overcome the aforementioned restrictions and provide a more accurate and comprehensive base for the CRAND study on Saturn.

2.2. GCR Tracing

GCR trajectory tracing is an extensively used method for the determination of the GCR access energies [*Smart and Shea*, 1994; *Selesnick*, 2002; *Kress et al.*, 2004; *Smart and Shea*, 2005; *Weygand and Raeder*, 2005; *Chu and Qin*, 2016; *Adriani et al.*, 2016]. The common approach is to launch particles from a given latitude and longitude sequentially at zenith angles from $-90°$ to $90°$ and at corresponding phase angles in order to cover the whole range of possible arrival directions, to trace these particles backwards in time and determine, if they escape the magnetosphere or not (here we set the borders of the magnetosphere at the radial distance of $25R_S$). Reversal in time implies that this particle can also enter the magnetosphere and hit the planet.

Figure 1 shows trajectories of five GCRs launched backwards in time from the top of Saturn's atmosphere. All five particles were launched from the same location and at the same pitch and phase angle, the only difference is their energy: 1 to 81 GeV. On this Figure it is seen, that only the 81-GeV particle can escape the magnetosphere, since its trajectory is "allowed", and the others are "forbidden", meaning the access energy for that given location and arrival direction is between 61 GeV and 81 GeV.

The ECPT (Energetic Charged Particle Tracing) code was developed especially for the purpose of this project and was validated using the Cassini MIMI/LEMMS observations during Rhea and Dione flybys [*Kotova et al.*, 2015]. As a magnetospheric model we used here the dipole model with a shift of the magnetic equator towards north by $0.036R_S$ and also the Khurana model, which today is the only global magnetospheric model of Saturn available to us [*Khurana et al.*, 2006]. It includes the internal spherical harmonic field, the ring currents and the magnetotail current system, the field from the radial current system, the shielding fields from the magnetopause and the interconnection magnetic field from the solar wind IMF. On the base of this model we performed simulations for different seasons: Pre-equinox (July 2004), Equinox (August 2009) and Post-Equinox (September 2017). As a numerical method for tracing of GeV particles we used the Vay method [*Vay*, 2008] - a modification of the Boris method [*Boris*, 1970] for relativistic particles, since it shows the best performance compared to the 4^{th}-order Runge-Kutta method and to the classical Boris scheme.

3. GCR Access Energies

3.1. Access Energy Mapped on Saturn

Figure 2 reports the GCR access energy mapped onto Saturn. Here the first row shows the simulation results based on the Dipole model and the second row - on the Khurana model for Equinox. The calculations were made assuming an isotropic distribution of 221 random arrival directions on every point on a grid of latitudes and longitudes.

Using semiempirical magnetospheric models, like the Khurana model, it is possible to resolve the diurnal variations in the magnetosphere, which is impossible using the dipole model. The deviation of the minimum access energies for latitudes below $\sim 60^\circ$ are within $\sim 8\%$. For the very high latitudes above $\sim 80^\circ$ there are already almost no variations because of the easier access there of the GCR particles, with trajectories almost parallel to the magnetic field lines. But for middle and high latitudes, between 60° and 80°, a significant local time variation in access energies is observed, especially for $70-75^\circ$ latitudes in both hemispheres. We found that at local midnight, the center of this map corresponding to, minimum access energy is 10 times (for 75° latitude) and 5 times (for 70° latitude) lower than at local noon regions. Figure 3 shows the deviation of the minimum access energy along latitudes from absolute minimum, centre of this map corresponds to local midnight.

Figure 4 shows the comparison of access energies obtained by the analytical Störmer approach (Westward, vertical and Eastward) and by using the particles tracing method, on the base of the Dipole model and of the Khurana model. Here it is clearly seen that, access energies depending on the arrival direction vary much more, than the analytical solution predicts. Störmer vertical cutoff energy, commonly used as a mean value for the GCR access energy, is significantly lower, than the numerically derived access energy sufficient for the half of the arriving directions. Particle tracing on the base of the Khurana model results in even bigger difference between analytically and numerically derived access energies.

3.1.1. Dipole model versus Khurana model

The Khurana magnetospheric model allows us to evaluate the GCR access to Saturn for different seasons, and the variation between various seasons will naturally depend on the accuracy of the particular model. Our comparison of GCR access during Preequinox and Equinox shows the difference in access energy around a few percent for most of the arrival directions on latitudes between $\sim 25^\circ$ and $\sim 60^\circ$ and up to $20-40\%$ for some arrival directions for latitudes $\sim 70^\circ$. Therefore depending on the studied problem these variations can be either ignored or taken into consideration.

Particle tracing on the base of a Dipole model results in GCR access energies, which differ by $20-80$ percent from the values obtained with the Khurana model for the majority of the arrival directions, and this difference increases towards high latitudes up to several times for some arrival directions. Herewith for low latitudes dipole model tracing results in higher access energies than using Khurana model, and for middle and high latitudes (above $\sim 20-25^\circ$) opposite. In absolute values the maximum difference is about $40-80$ GeV for some directions. Since significant difference is found on all latitudes, it suggests, that the calculations on the base of realistic magnetospheric models are more preferable. The values of access energies for various fractions of the arriving directions calculated on the base of the Khurana model demonstrated on Figure 4 can be found in Table S3 in the Supporting Information.

3.1.2. Impact of the Main Rings

Another important aspect in the evaluation of the GCR interaction with Saturn is the rings crossing rate. Every time the GCR particle crosses the rings it might stop or lose some of its energy, changing its trajectory. Moreover, every passage through the rings will produce a cascade of secondaries, triggering the CRAND process.

We calculated the percentage of particles per number of ring crossings averaged across longitudes for different latitudes. It can be noticed, that at latitudes below $\sim 35^{\circ}$, in both hemispheres, most of the allowed trajectories cross the rings at least 3 times on their way. And for middle latitudes ($\sim 40^{\circ}$) for some very few arrival directions particles can cross the rings up to 12 times. For the current study the assumption is, that a GeV-particle does not lose energy when crossing the rings, but in reality particles either stop or lose a few percent of their energy per crossing, depending on the thickness of the rings. The ring crossing rate should be taken into account in the estimation of the GCR flux at lower latitudes of Saturn and for the evaluation of the CRAND production rate.

To illustrate the possible impact of the non-transparent rings we calculated GCR access energies assuming that particle lose 50% of its energy in every passage through the rings (determined at a distance from the centre of the planet 66 900 km - 140 180 km). On the upper panel of Figure 5 on top of the already shown in Figure 4 access energies in fractions of the arrival directions we plot contours, which shows access energy sufficient for the same portion of the arrival directions, but obtained with assumption, that rings are not transparent. Dashed green line highlights the access energy for the 50% of the arrival directions and dash-point red line - minimum access energy. On the bottom panel we show

for how much percent increases access energy for every fraction. Here we see, that access energy for half of arrival directions increases for $40-60\%$ at the middle and low latitudes, minimum access energy increases only for few percent and the ultimate access energy, which assure that particles can arrive from every direction, increases up to several times, depending on the latitude. More precise calculation of the rings impact on the GCR access to the Saturnian atmosphere considering different scenarios is left for the future work.

3.1.3. East-West asymmetry

The predicted by *Rossi* [1930] so-called "East-West effect" occurs also at Saturn, but in reversed direction compared to the Earth, because of the opposite orientation of the magnetic moment of the planet dipole. The access energy depends on the arrival direction. To reach the point at the top of the atmosphere from the west the GCR should have much more energy, than from the east, and the difference is bigger at lower latitudes. For instance, the 65 GeV GCR managed to arrive to equator from the east, while from the west the allowed trajectories started only from 350 GeV, since the planet shadows the lower energy trajectories. This example is depicted on the upper panel of Figure 6.

The bottom panel of Figure 6 demonstrates the dependence of the access energy on arrival direction for different latitudes. The arrival direction at Saturn's surface in local horizon coordinates can be described by two angles: azimuth (Az, from 0°0 to 360°) and zenith (Zen, from 0° to 90°). Therefore for the projection to the plane $x = cos(Az)sin(Zen)$ and $y = sin(Az)sin(Zen)$. For instance, for North those angles would be $Zen = 90°$ and $Az = 0°$. Here each point corresponds to one of 221 arrival directions. More reddish

points indicate higher access energy for this particular arrival direction for the current latitude.

3.2. Access Energies to the Saturn's Magnetosphere

We used the same approach to evaluate the GCR access to the equatorial plane of the magnetosphere, which can uncover the intensity of the GCR interaction with the Saturnian rings, neutral gas cloud and moons. One may also use these results to understand how easily ions from ICME events may populate the magnetosphere [*Roussos et al.*, 2018b]. The trajectory tracing was performed from points located at distances from $1.05R_S$ (Saturn radii) up to $20R_S$ from Saturn towards the Sun in the equatorial plane. For every point 211 arrival directions were evaluated. Figure 7 reports the modeling results on the basis of the Dipole model (upper panel) and the Khurana model for Preequinox. The different contours represent the fractions of allowed arrival directions as a function of energy and distance from the planet. The grey zone indicates the location of the Main Rings and is zoomed in separately on Figure S2 in Support Information. Also these values are available in the Table S4 in the Supporting Information. It should be noted, that some of the arrival directions produce extremely high access energy values in the close vicinity to the planet, since we evaluated them isotropically distributed in a whole volume of incidence angles and about the half of arrival directions very close to the planet are simply forbidden because of the presence of the planet.

The biggest difference in the two plots at Figure 7 can be observed at distances outside 7 R_S, since the dipole model can well describe the equatorial magnetic field only close to Saturn. Here values for GCR access energy on the base of the Khurana model are about

twice lower for the same arrival directions. The values of access energies for various fractions of the arriving directions calculated on the base of the Khurana model demonstrated on bottom panel of Figure 7 can be found in Table S5 in the Supporting Information.

4. GCR Spectra and Integral Flux

The fractional distribution allows reconstruction of the GCR spectra at Saturn. Due to lack of detailed GCR measurements on Saturn we used, as a parent (before entering into the magnetosphere) GCR spectrum, the estimation of a general GCR flux on that distance from the Sun. For that the CREME (Cosmic Ray Effects on Micro-Electronics code) data for general GCR spectra in the vicinity of the Earth [*Tylka et al.*, 1997; *Weller et al.*, 2010; *Mendenhall and Weller*, 2012] were multiplied by a factor of 1.425 in order to take into account the radial gradient of 5% per AU [*McDonald et al.*, 1997]. By applying the GCR fraction distribution, one can model the GCR spectra to the particular location on the planet or in the magnetosphere. Upper left panel of Figure 8 shows the initial (parent) GCR spectrum and the obtained modeled spectra, averaged along every 5° of latitudes. Upper right panel demonstrates the modeled GCR spectra for radial distances up to 20 R_S from the planet. For the evaluation of the CRAND production rate from the Main Rings, the fluxes corresponding to the radial distances of the rings are most important, therefore we marked the spectra at the distances of the D-ring (innermost ring) and the F-ring (the outermost ring). These spectra can be used directly as an input for the evaluation of the CRAND production rate, noting however that they do not include effects from GCR multiple ring crossings. These spectra can be found in the Support Information.

Using the modeled GCR spectra it might be interesting to calculate the GCR integrated flux, which is shown on the lower left panel of Figure 8 for the atmosphere of Saturn and on the lower right panel for the equatorial plane of the magnetosphere. These results based on simulations using the Khurana model for Preequinox and Equinox. The decrease in the integrated flux at the atmosphere towards the equatorial zone is a direct consequence of an increase in the access energy at the corresponding latitudes, demonstrated in Figure 2. Here the differences in the two flux levels for different seasons arise from differences in initial GCR fluxes for these particular solar cycle phases.

On Figure 8 it is seen that the integral GCR flux to the rings and atmosphere below $\sim 70^{\circ}$ is independent of solar cycle phases, which supports the *Kollmann et al.* [2017] results saying that variations in radiation belts have to come from other processes, e.g. diffusion.

As it was reported by *Roussos et al.* [2018b] the background GCR noise in the various channels of the Cassini MIMI/LEMMS instrument decreased notably during the close approach to the planet. On panel D) of Figure 8 we compared the LEMMS E7 count rates from Saturn Orbit Insertion (SOI) normalized to integral flux at $12R_S$, with the integrated above 300 MeV modeled flux profile for Preequinox. The E7 data are shown with red diamonds. The point at $L = 1$ (orange diamond) is the "1 count upper limit" inside $L = 1.03$, assuming that 1 count would have been counted in the total 600 sec that Cassini spent inward of that region. In reality, during the Proximal orbits channel E7 measured 0 counts, consistent with our prediction of even lower GCR fluxes than the 1

count upper limit. The drop in the GCR noise in LEMMS measurements starts developing at about 6 Rs, as predicted in the simulations, and is proportional to our modeled and integrated GCR flux dropout in the close vicinity of Saturn, which supports the idea of GCR origin of this background signal.

5. Summary

The MeV proton radiation belts of Saturn are proved to be isolated from the outer magnetosphere, and the source of these high energy protons should be related to the GCRs. Therefore a realistic flux of GCRs in the Saturnian system is required and, in this letter, we propose a numerical solution for the calculation of the GCR access energies to Saturnian magnetosphere and demonstrate its advantage over the analytical approach.

While to a first order, the Störmer theory predicts well the access of GCRs at the rings and the low latitude atmosphere, depending on the accuracy of the problem studied, this approximation may be less or more appropriate. Since, for instance, LEMMS measurements indicate that CRAND is a very well defined and quasi-stable process at Saturn, the results from particle tracing will be important for reducing the small but non-negligible errors introduced by the analytical theory, if we want to reconstruct the CRAND spectra with good precision.

As a result we obtained the GCR access energies to the atmosphere of the planet and its rings, using two different magnetospheric models: a Dipole model and the Khurana model. We demonstrate that numerical solution provides more detailed information about

the GCR access energies, and is more preferable for future usage than the Störmer vertical cutoff as a mean value.

We analysed the variations of the access energy in many different aspects and calculated the GCR spectra and GCR integrated flux to the atmosphere of Saturn as a function of latitude, and to the equatorial distance of the Saturnian magnetosphere as a function of distance from the planet.

Having determined the incoming GCR flux, it is possible now to perform a simulation of the cascades of particles resulting from GCR penetration through the rings and GCR impact on the Saturn's atmosphere, and to calculate the CRAND input to the ion populations of the radiation belts.

Acknowledgments. The authors like to thank K. Khurana for the magnetospheric model code and L. Regoli for the help with a particle tracing code. Funding was provided by CNES (AK, ID), German BMWi through the German Space Agency DLR under contracts 50OH0103, 50OH0801, 50OH0802, 50OH1101, 50OH1502 and by the Max Planck Society (AK, IR, NK). PK was partially supported by the NASA Office of Space Science under task order 003 of contract NAS5-97271 between NASA/GSFC and JHU. The Cassini/MIMI data are available through NASA's Planetary Data System at https://pdsppi.igpp.ucla.edu/mission/Cassini-Huygens/CO/MIMI.

In the Supporting Information we provide the look-up tables with GCR access energies to the planet and to the equatorial plane of the magnetosphere, calculated on the base of the Khurana model, the modeled GCR spectra as a function of latitude and as a function of distance from Saturn. Also we provide some details about the Störmer cutoff rigidities calculation and additional figures demonstrating changes in the minimum access energy along latitudes and showing GCR access energies to Saturnian rings.

References

Adriani, O., G. C. Barbarino, G. A. Bazilevskaya, R. Bellotti, M. Boezio, E. A. Bogomolov, M. Bongi, V. Bonvicini, S. Bottai, A. Bruno, F. Cafagna, D. Campana, P. Carlson, M. Casolino, G. Castellini, C. De Donato, G. A. de Nolfo, C. De Santis, N. De Simone, V. Di Felice, A. M. Galper, A. V. Karelin, S. V. Koldashov, S. Koldobskiy, S. Y. Krutkov, A. N. Kvashnin, A. Leonov, V. Malakhov, L. Marcelli, M. Martucci, A. G. Mayorov, W. Menn, M. Mergé, V. V. Mikhailov, E. Mocchiutti, A. Monaco, N. Mori, R. Munini, G. Osteria, F. Palma, B. Panico, P. Papini, M. Pearce, P. Picozza, M. Ricci, S. B. Ricciarini, R. Sarkar, V. Scotti, M. Simon, R. Sparvoli, P. Spillantini, Y. I. Stozhkov, A. Vacchi, E. Vannuccini, G. I. Vasilyev, S. A. Voronov, Y. T. Yurkin, G. Zampa, and N. Zampa (2016), PAMELA's measurements of geomagnetic cutoff variations during the 14 December 2006 storm, *Space Weather*, *14*(3), 210–220, doi:10.1002/2016SW001364, 2016SW001364.

Beer, J., K. McCracken, and R. von Steiger (2012), *Geosphere*, pp. 369–388, Springer Berlin Heidelberg, Berlin, Heidelberg, doi:10.1007/978-3-642-14651-0_21.

Blake, J. B., H. H. Hilton, and S. H. Margolis (1983), On the injection of cosmic ray secondaries into the inner saturnian magnetosphere: 1. protons from the crand process, *Journal of Geophysical Research: Space Physics*, *88*(A2), 803–807.

Boris, J. P. (1970), Relativistic plasma simulation - optimization of a hybrid code, *Proceeding of Fourth Conference on Numerical Simulations of Plasmas*.

Chu, W., and G. Qin (2016), The geomagnetic cutoff rigidities at high latitudes for different solar wind and geomagnetic conditions, *Annales Geophysicae*, *34*(1), 45–53, doi: 10.5194/angeo-34-45-2016.

Cooper, J. F. (1983), Nuclear cascades in saturn's rings: Cosmic ray albedo neutron decay and origins of trapped protons in the inner magnetosphere, *Journal of Geophysical Research: Space Physics*, *88*(A5), 3945–3954.

Cooper, J. F., J. H. Eraker, and J. A. Simpson (1985), The secondary radiation under saturn's a-b-c rings produced by cosmic ray interactions, *Journal of Geophysical Research: Space Physics*, *90*(A4), 3415–3427.

Dorman, L. (2009), *Cosmic Rays in Magnetosphere of the Earth and other Planets*, Springer Netherlands.

Fillius, W., and C. McIlwain (1980), Very energetic protons in Saturn's radiation belt, *Journal of Geophysical Research Space Physics*, *85*(A11), 5803–5811.

Fillius, W., W. H. Ip, and C. E. McIlwain (1980), Trapped radiation belts of Saturn: First look, *Science*, *207*(4429), 425–431.

Kallenrode, M.-B. (2004), *Space Physics. An Introduction to Plasmas and Particles in the Heliosphere and Magnetospheres*, 3rd ed., Springer-Verlag Berlin Heidelberg.

Khurana, K. K., C. S. Arridge, H. Schwarzl, and M. K. Dougherty (2006), A Model of Saturn's Magnetospheric Field Based on Latest Cassini Observations, *AGU Spring Meeting Abstracts*.

Kollmann, P., E. Roussos, A. Kotova, L. Regoli, D. G. Mitchell, J. Carbary, G. Clark, N. Krupp, and C. Paranicas (2018), Saturn's innermost radiation belt throughout and inward of the d-ring, *Geophysical Research Letters*, *45*, 10,912–10,920. doi: 10.1029/2018GL077954.

Kollmann, P., E. Roussos, C. Paranicas, N. Krupp, and D. Haggerty (2013), Processes forming and sustaining Saturn's proton radiation belts, *Icarus*, *222*(1), 323 – 341.

Kollmann, P., E. Roussos, A. Kotova, C. Paranicas, and N. Krupp (2017), The evolution of saturn's radiation belts modulated by changes in radial diffusion, *Nature Astronomy*, *1*(12), 872–877, doi:10.1038/s41550-017-0287-x.

Kotova, A., E. Roussos, N. Krupp, and I. Dandouras (2015), Modeling of the energetic ion observations in the vicinity of Rhea and Dione, *Icarus*, *258*, 402 – 417.

Kress, B. T., M. K. Hudson, K. L. Perry, and P. L. Slocum (2004), Dynamic modeling of geomagnetic cutoff for the 23-24 November 2001 solar energetic particle event, *Geophysical Research Letters*, *31*(4), doi:10.1029/2003GL018599, l04808.

Krimigis, S. M., and T. P. Armstrong (1982), Two-component proton spectra in the inner Saturnian magnetosphere, *Geophysical Research Letters*, *9*(10), 1143–1146.

McDonald, F. B., P. Ferrando, B. Heber, H. Kunow, R. McGuire, R. Ḿuller-Mellin, C. Paizis, A. Raviart, and G. Wibberenz (1997), A comparative study of cosmic ray radial and latitudinal gradients in the inner and outer heliosphere, *Journal of Geophysical Research: Space Physics*, *102*(A3), 4643–4651, doi:10.1029/96JA03673.

Mendenhall, M. H., and R. A. Weller (2012), A probability-conserving cross-section biasing mechanism for variance reduction in monte carlo particle transport calculations, *Nuclear Instruments and Methods in Physics Research Section A: Accelerators, Spectrometers, Detectors and Associated Equipment*, *667*, 38 – 43.

Nakamura, K., and P. D. Group (2010), Review of particle physics, *Journal of Physics G Nuclear and Particle Physics*, *37*(7A), 075,021.

Paranicas, C., D. Mitchell, S. Krimigis, D. Hamilton, E. Roussos, N. Krupp, G. Jones, R. Johnson, J. Cooper, and T. Armstrong (2008), Sources and losses of energetic protons in Saturn's magnetosphere, *Icarus*, *197*(2), 519 – 525.

Randall, B. A. (1994), Energetic electrons in the magnetosphere of Saturn, *Journal of Geophysical Research: Space Physics*, *99*(A5), 8771–8785.

Reid, G. C., and H. H. Sauer (1967), The influence of the geomagnetic tail on low-energy cosmic-ray cutoffs, *Journal of Geophysical Research*, *72*(1), 197–208, doi: 10.1029/JZ072i001p00197.

Rossi, B. (1930), On the magnetic deflection of cosmic rays, *Physical Review*, *36*, 606–606, doi:10.1103/PhysRev.36.606.

Roussos, E., N. Krupp, T. P. Armstrong, C. Paranicas, D. G. Mitchell, S. M. Krimigis, G. H. Jones, K. Dialynas, N. Sergis, and D. C. Hamilton (2008), Discovery of a transient radiation belt at Saturn, *Geophysical Research Letters*, *35*(22).

Roussos, E., N. Krupp, C. P. Paranicas, P. Kollmann, D. G. Mitchell, S. M. Krimigis, T. P. Armstrong, D. R. Went, M. K. Dougherty, and G. H. Jones (2011), Long- and short-term variability of Saturn's ionic radiation belts, *Journal of Geophysical Research: Space Physics*, *116*(A2), a02217.

Roussos, E., P. Kollmann, N. Krupp, A. Kotova, L. Regoli, C. Paranicas, D. G. Mitchell, S. M. Krimigis, D. Hamilton, P. Brandt, J. Carbary, S. Christon, K. Dialynas, I. Dandouras, M. E. Hill, W. H. Ip, G. H. Jones, S. Livi, B. H. Mauk, B. Palmaerts, E. C. Roelof, A. Rymer, N. Sergis, and H. T. Smith (2018a), A radiation belt of energetic protons located between saturn and its rings, *Science*, *362*(6410), doi: 10.1126/science.aat1962.

Roussos, E., C. Jackman, M. Thomsen, W. Kurth, S. Badman, C. Paranicas, P. Kollmann, N. Krupp, R. Bučík, D. Mitchell, S. Krimigis, D. Hamilton, and A. Radioti (2018b), Solar energetic particles (sep) and galactic cosmic rays (gcr) as tracers of solar wind conditions near saturn: Event lists and applications, *Icarus*, *300*, 47 – 71, doi:https://doi.org/10.1016/j.icarus.2017.08.040.

Selesnick, R. S. (2002), Cosmic ray access to Jupiter's magnetosphere, *Geophysical Research Letters*, *29*(9), 12–1–12–4, doi:10.1029/2001GL014146.

Simpson, J. A., T. S. Bastian, D. L. Chenette, G. A. Lentz, R. B. McKibben, K. R. Pyle, and A. J. Tuzzolino (1980), Saturnian trapped radiation and its absorption by satellites and rings: The first results from Pioneer 11, *Science*, *207*(4429), 411–415.

Smart, D., and M. Shea (1994), Geomagnetic cutoffs: A review for space dosimetry applications, *Advances in Space Research*, *14*(10), 787 – 796, doi: http://dx.doi.org/10.1016/0273-1177(94)90543-6.

Smart, D., and M. Shea (2005), A review of geomagnetic cutoff rigidities for earth-orbiting spacecraft, *Advances in Space Research*, *36*(10), 2012 – 2020, doi:http://dx.doi.org/10.1016/j.asr.2004.09.015, solar Wind-Magnetosphere-Ionosphere Dynamics and Radiation Models.

Tylka, A. J., J. H. Adams, P. R. Boberg, B. Brownstein, W. F. Dietrich, E. O. Flueckiger, E. L. Petersen, M. A. Shea, D. F. Smart, and E. C. Smith (1997), CREME96: A Revision of the Cosmic Ray Effects on Micro-Electronics Code, *IEEE Transactions on Nuclear Science*, *44*, 2150–2160+.

Van Allen, J. A., B. A. Randall, and M. F. Thomsen (1980), Sources and sinks of energetic electrons and protons in Saturn's magnetosphere, *Journal of Geophysical Research Space Physics*, *85*(A11), 5679–5694.

Vay, J.-L. (2008), Simulation of beams or plasmas crossing at relativistic velocity, *Physics of Plasmas*, *15*(5), 056701.

Vogt, R. E., D. L. Chenette, A. C. Cummings, T. L. GARRARD, E. C. Stone, A. W. Schrdt, J. H. Trainor, N. Lal, and F. B. McDonald (1982), Energetic charged particles in Saturn's magnetosphere: Voyager 2 results, *Science*, *215*(4532), 577–582.

Weller, R., M. Mendenhall, R. Reed, R. Schrimpf, K. Warren, B. Sierawski, and L. Massengill (2010), Monte carlo simulation of single event effects, *Nuclear Science, IEEE Transactions on*, *57*(4), 1726–1746.

Weygand, J. M., and J. Raeder (2005), Cosmic ray cutoff prediction using magnetic field from global magnetosphere MHD simulations, *Annales Geophysicae*, *23*(4).

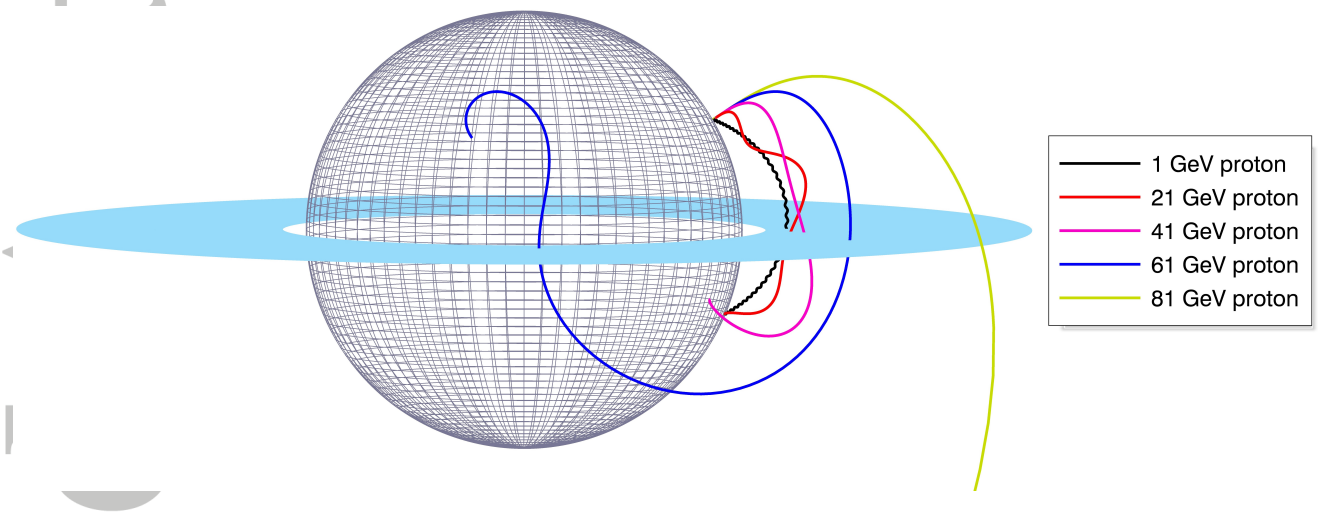

Figure 1. Simulated backwards in time trajectories of five protons of different energies. Only the 81-GeV proton has an allowed trajectory and will escape the magnetosphere, while the other particles hit the planet: their trajectories are forbidden.

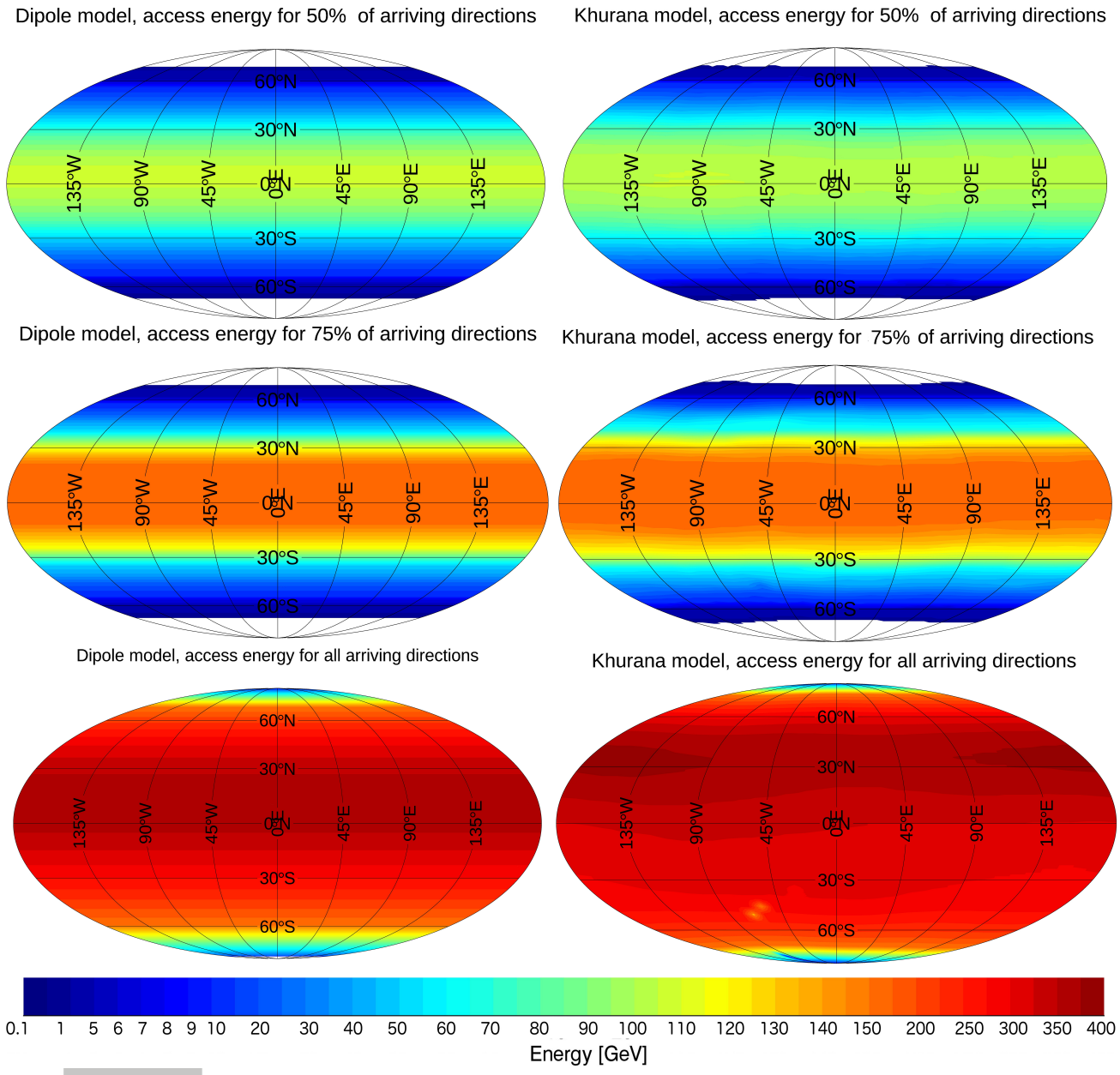

Figure 2. GCR access energy mapped to Saturn using the Dipole model (left column) and the Khurana model (right column). The three rows give the access energy for different portions of arrival directions (the first row - energy needed for 50% of the arrival directions, the second row - energy needed for 75% of the arrival directions, and the third row - ultimate access energy, covering all arrival directions). Zero longitude corresponds to the local midnight.

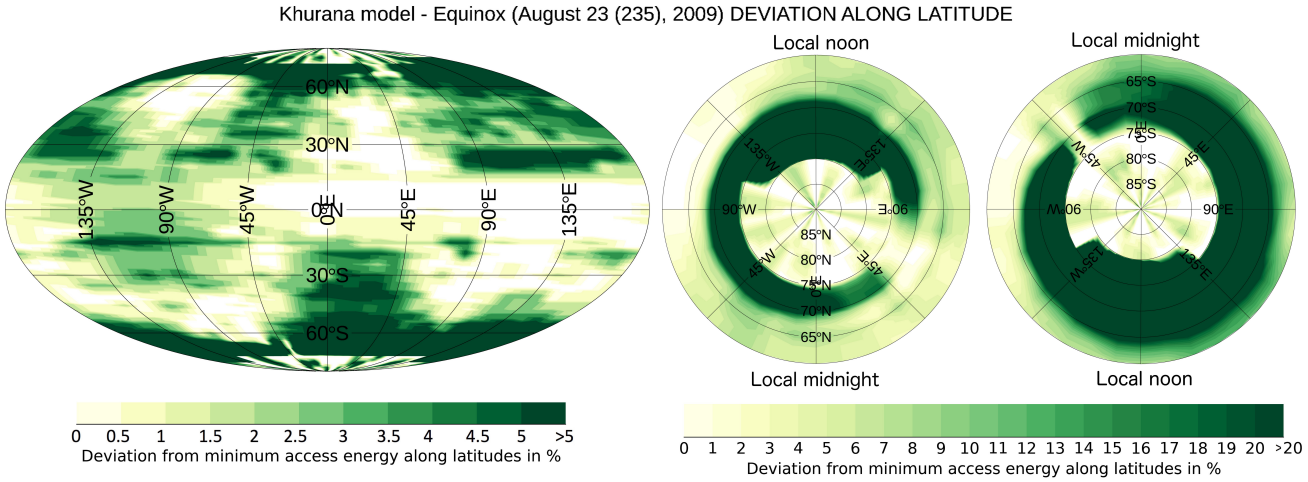

Figure 3. GCR access energy to Saturn: deviation of minimum access energy along latitudes, calculated using Khurana model. Polar regions are shown separately on the right panel. Zero longitude corresponds to the local midnight.

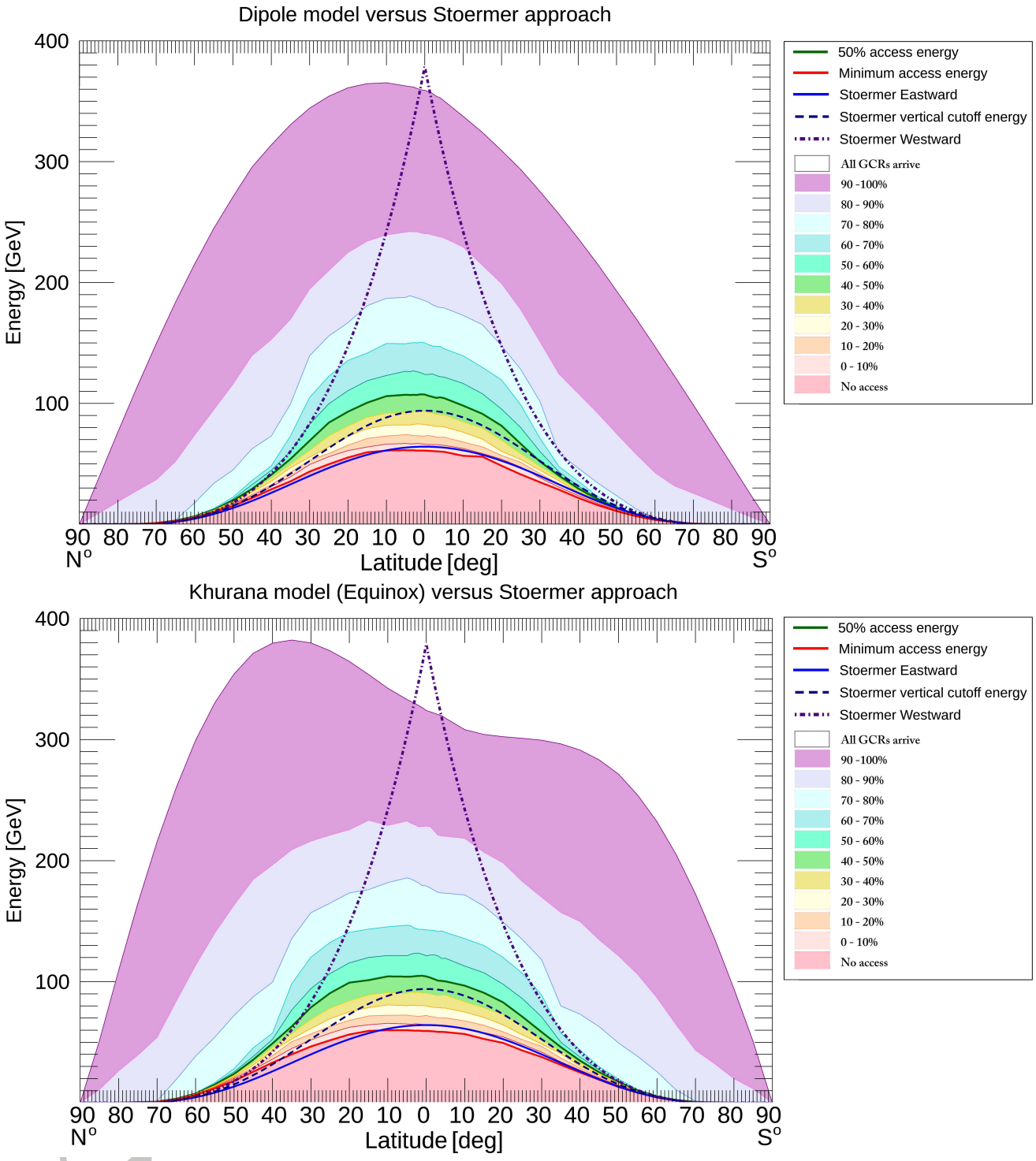

Figure 4. GCR access energy in fractions of arrival directions as a function of energy and latitude, in comparison with Störmer cutoff energies: Westward (point-dash indigo line), vertical (dashed navy line) and Eastward (solid blue line). Contours represent the different fractions of allowed arrival directions, obtained by particle tracing, the solid red line highlights the absolute minimum access energy, the solid green line - energy needed for 50% of arrival directions.

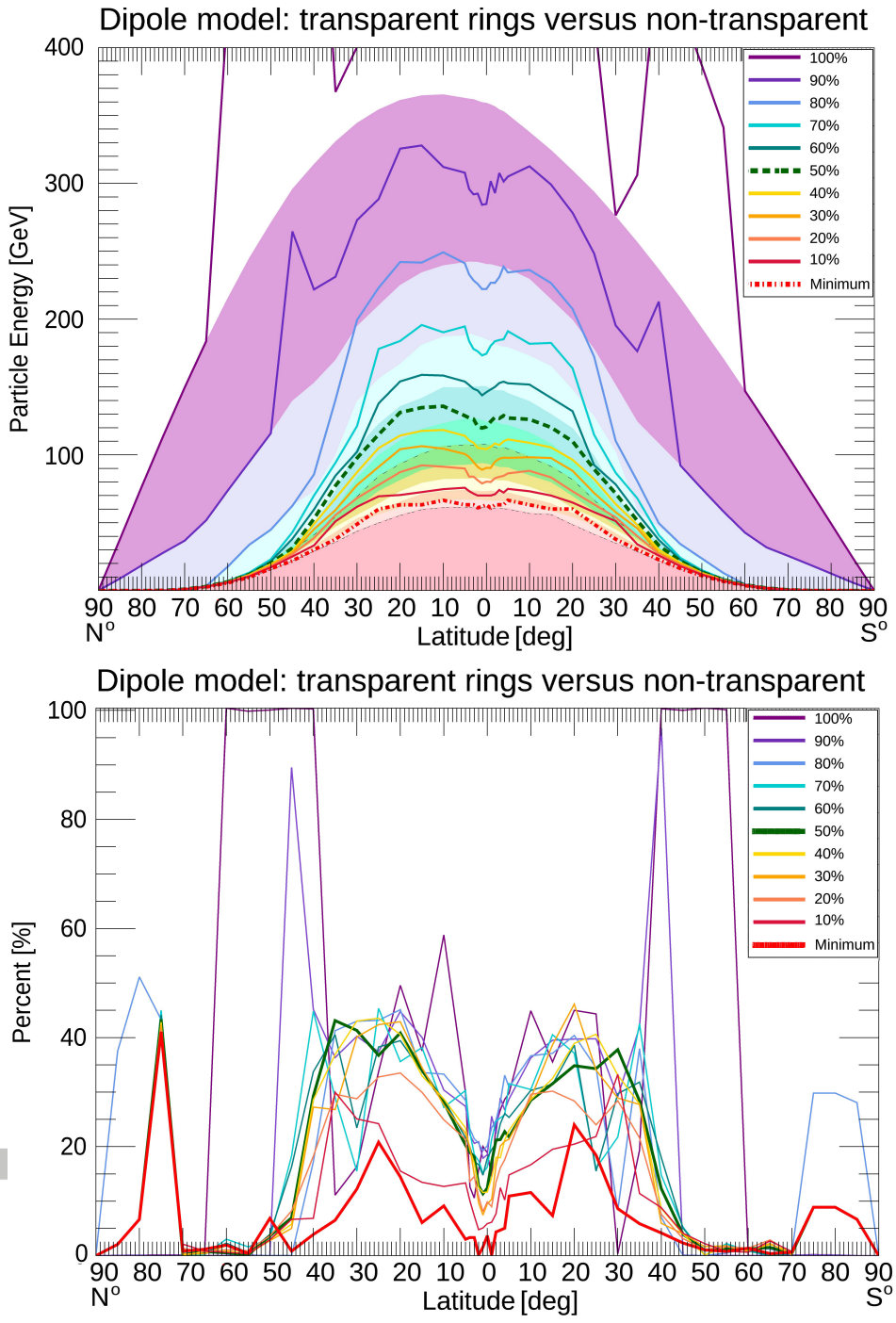

Figure 5. Changes in the GCR access energy if rings are not transparent for particles. Upper panel: GCR access energy in fractions of arrival directions as a function of energy and latitude calculated assuming rings are transparent for GCRs (solid coloured zone) and contours of the same colour indicate, how the access energy for corresponding fraction of arrival directions will increase, if we assume GCR lose 50% of its energy in every passage through the rings. Bottom panel: percentage of the GCR access energy increase for corresponding fractions of arrival directions if the rings assumed not transparent as a function of latitude.

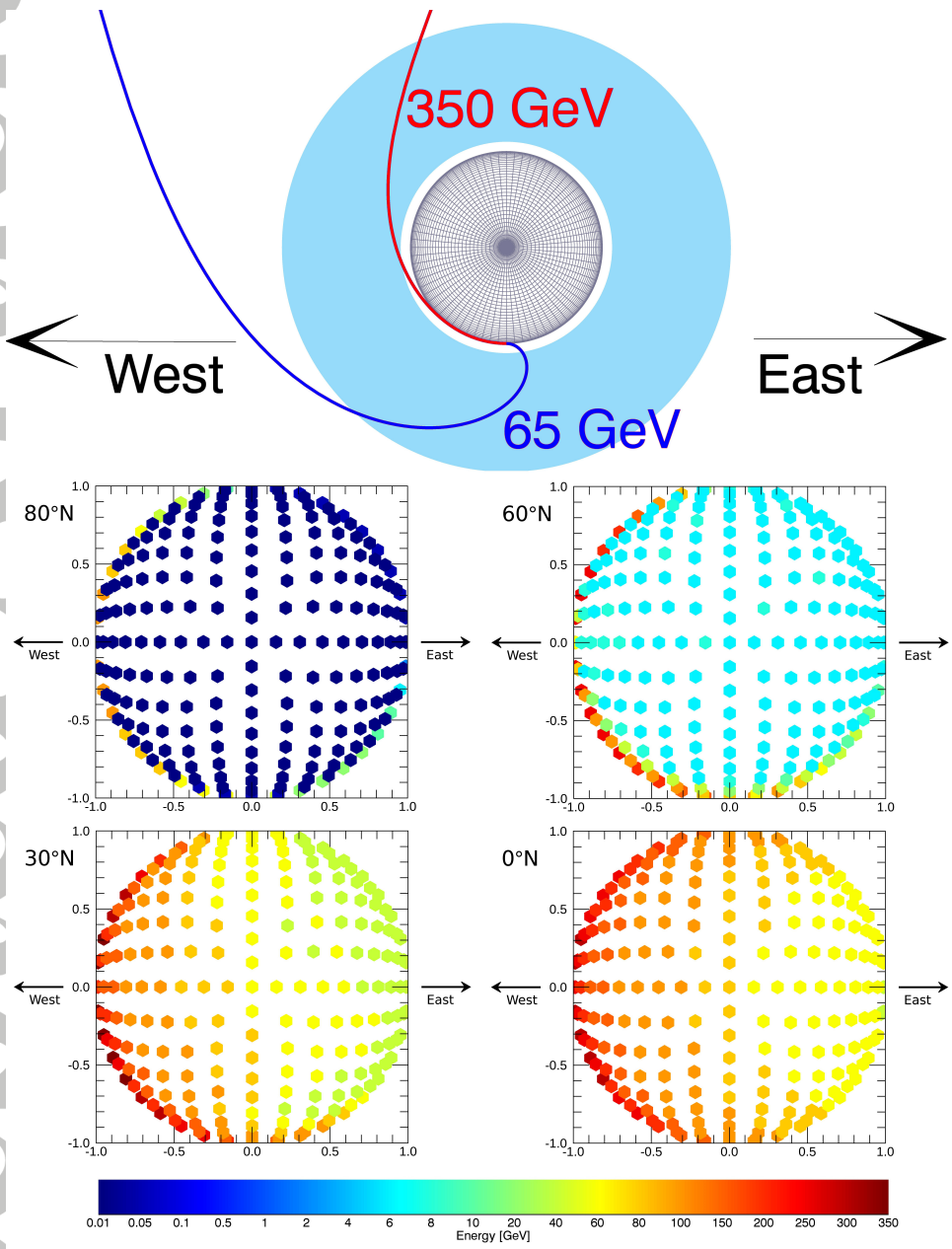

Figure 6. Minimum access energy per arrival direction for different latitudes. X-axis is the cosine and y-axis is the sine of the arrival direction. West is on the left and East on the right.

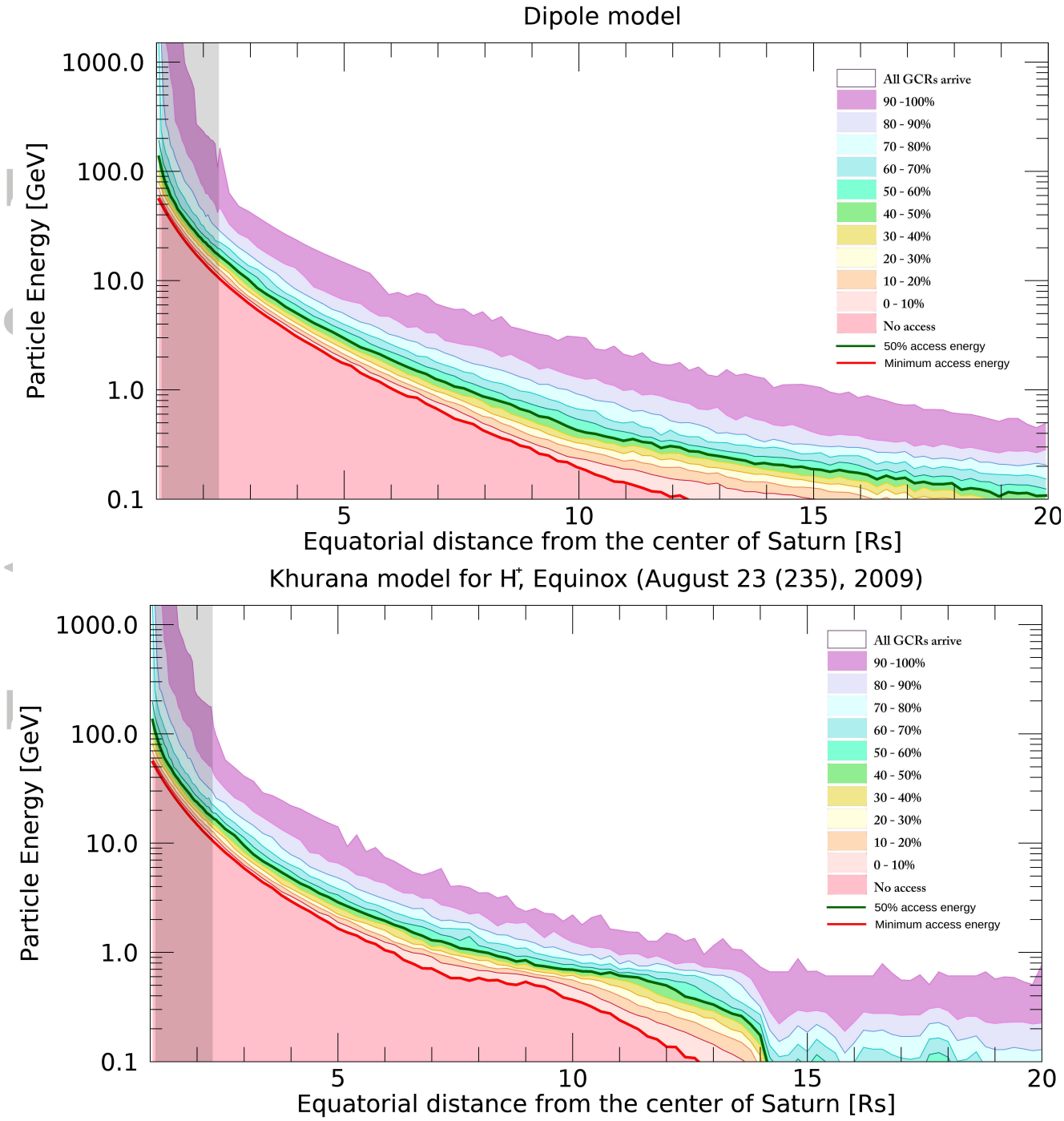

Figure 7. GCR proton access energy in fractions of arrival directions as a function of energy and distance from the planet (Rs - is the Saturn radii) in the equatorial plane: comparison between the Dipole model (upper panel) and Khurana model for Preequinox (lower panel). The location of the Main Rings is indicated by the grey zone. Different contours represent fractions of arrival directions as a function of access energy, a pink zone indicates no access of particles with such energy to the corresponding point and a white zone indicates the full access to the point from all arrival directions.

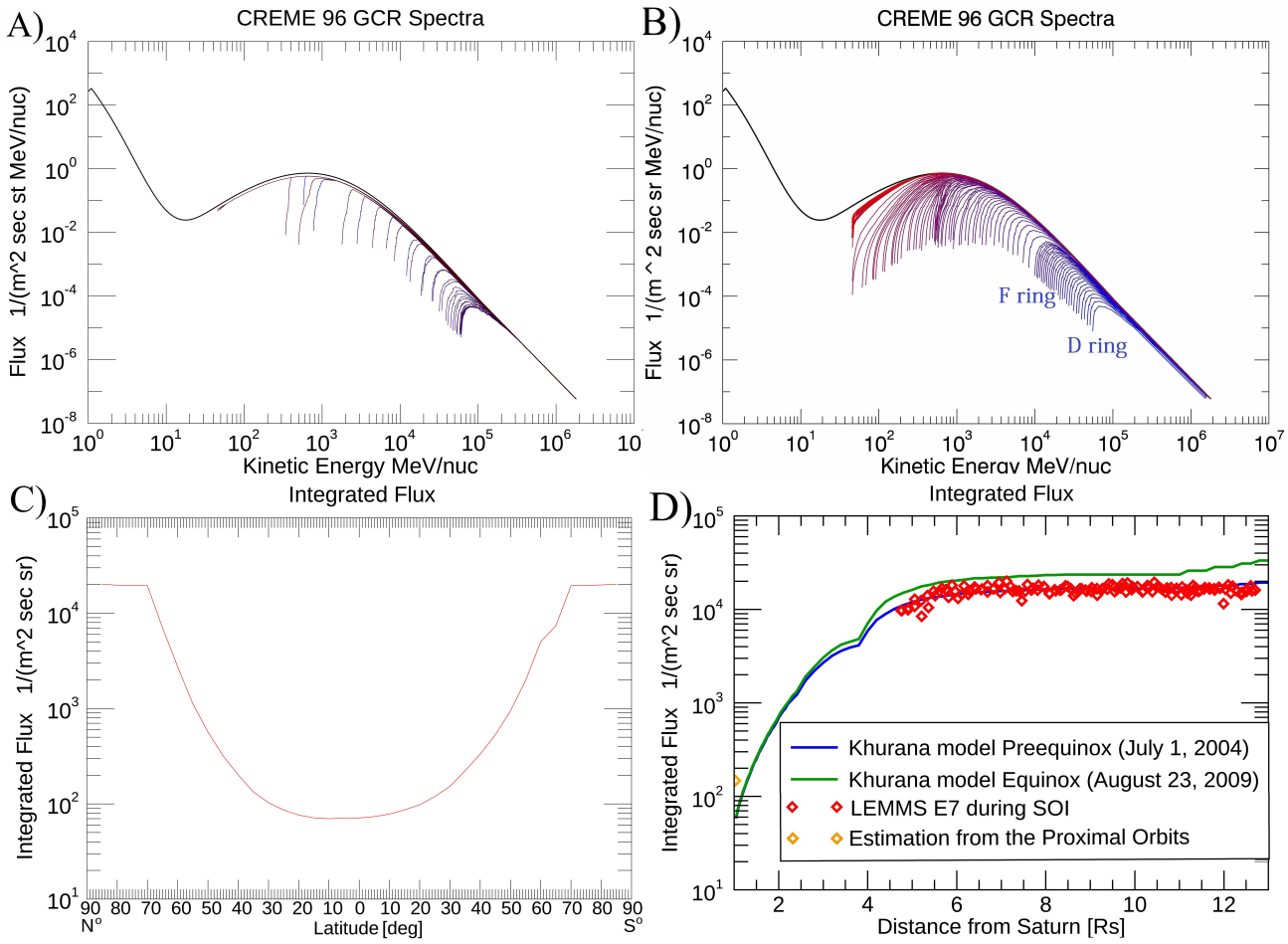

Figure 8. Panel (A): The estimated GCR spectra in the vicinity of Saturn and modeled spectra for different latitudes (on the base of Khurana model, Preequinox). Panel (B): The modeled GCR spectra (on the base of the Khurana model, Preequinox) as a function of distance from Saturn [R_S]. Panel (C): The modeled GCR integrated fluxes above the minimum access energy per latitude, using the Khurana model for Equinox. Panel (D): The modeled GCR integrated fluxes as a function of distance from Saturn [R_S], using the Khurana model for Preequinox and Equinox, and for comparison the Cassini LEMMS calibrated E7 count rates during SOI, normalised to the total flux.